Journal of Coordination Chemistry

Iron(III) complexes with 2-aminobenzothiazole: compounds governed by non-covalent interactions

Agata Trzesowska-Kruszynska [a]

[a] Department of X-Ray Crystallography and Crystal Chemistry,
Institute of General and Ecological Chemistry, Technical University
of Lodz, Zeromskiego 116, 90-924 Lodz, Poland
Published online: 04 Feb 2011.

PLEASE SCROLL DOWN FOR ARTICLE

Taylor & Francis
Taylor & Francis Group

Iron(III) complexes with 2-aminobenzothiazole: compounds governed by non-covalent interactions

AGATA TRZESOWSKA-KRUSZYNSKA*

Department of X-Ray Crystallography and Crystal Chemistry, Institute of General and Ecological Chemistry, Technical University of Lodz, Zeromskiego 116, 90-924 Lodz, Poland

Two new iron(III) coordination compounds with 2-aminobenzothiazole have been prepared and identified as $(C_6H_4NHC(NH_2)S)_2[FeCl_4]Cl(H_2O)$ (**1**) and $(C_6H_4NHC(NH_2)S)_3$ $[Fe(C_2O_4)_3](H_2O)_2$ (**2**). The compounds were characterized by thermogravimetric analysis in conjunction with evolved gases in air and spectroscopic studies. On the basis of quantum-mechanical calculations the interplay between two non-covalent interactions in **1**, anion$\cdots\pi$ and ion-pair interactions, was analyzed.

Keywords: 2-Aminobenzothiazolium; Anion-π interactions; Bond-valence method; NBO analysis; Thermal decomposition

1. Introduction

Design and preparation of host/receptor molecules binding anionic entities has attracted attention [1–4]. Anion recognition is important due to its potential applications in medicine, catalysis, environmental protection, separation processes, and biomolecular systems. Positively charged or neutral receptors bind anions by different types of non-covalent interactions, hydrogen bonds, electrostatic interactions [5], or coordination bonds for metal/metalloid–macrocyclic complexes acting as host molecules [6–8]. In comparison to cationic receptors, neutral receptors do not require the presence of the charge-balancing counterions. The neutral receptors are also more selective due to the directionality of the interactions.

Compounds designed to target anions should be selective and strongly bind anionic moieties. The strength of interactions is important due to anion solvation taking place in polar solvents, thus the receptor must efficiently compete with the solvent molecules [2]. Anions are large and require larger host cavities than cations. Energetically, the anion-binding interaction is less favorable due to larger equilibrium distances. The positively charged or neutral receptor molecules designed to non-covalently bind anionic guest species are based on polyamines, polyguanidinium cations, porphyrins, or sapphyrins. The energy of interaction can be increased either by increasing the number of binding interactions of one type, e.g. hydrogen bonds *via* incorporating additional

---

*Email: agata.trzesowska@p.lodz.pl

hydrogen-bond donors and acceptors [5, 9], or by combining different types of non-covalent interactions [2]. Recently, a new type of non-covalent interaction, anion $\cdots \pi$ interactions [10], has been considered as an alternative way of complexing anionic guests by neutral hosts.

Among the non-covalent interactions, anion $\cdots \pi$ interactions [11–14] are the least known and investigated. The existence of this type of interaction was neglected due to its expected repulsive character. In recent years, energetically favorable anion $\cdots \pi$ interactions have been evidenced by theoretical studies performed on simple model systems. Quantum-mechanical calculations show that anion $\cdots \pi$ interactions are dominated by electrostatic and polarization contributions and they are weaker than cation $\cdots \pi$ interactions and stronger than halogen bonds [15]. Crystallographic examples of these non-covalent interactions were presented and described in 2004 [16].

Generally, anion $\cdots \pi$ interactions are believed to occur between electron-donating anions and π-electron-poor aromatic moieties possessing positive molecular quadrupole moment [17]. However, recent theoretical studies indicate that aromatic rings with negative quadrupole moments can also form anion $\cdots \pi$ interactions [18], and even non-electron-deficient aromatic molecules are capable of binding anions when the aromatic ring is simultaneously interacting with a cation on the opposite face of the ring (anion $\cdots \pi \cdots$ cation) [19]. Both theoretical and experimental investigations have been carried out mainly for the systems containing inorganic anions, for example halide and nitrate, and neutral six-membered aromatic rings, such as halogenobenzene derivatives or s-triazine derivatives.

Neutral electron-deficient aromatic compounds, serving as potential receptor-binding anions *via* anion $\cdots \pi$ contacts, are highly selective, but the strength of interaction of about 5–20 kcal mol^{-1} (measured for idealized geometry in gas phase) [12, 20] can be too small to allow anion recognition in some systems. The strength of this interaction can be increased by increasing the anion–π system size (using dendritic ligands based on s-triazine ring [21, 22] or N-confused porphyrins [23]) and, consequently, by increasing the number of binding interactions or by incorporating additional non-covalent interactions. Similar combination of interactions including cation $\cdots \pi$, hydrophobic, and salt-bridge was applied to improve the cation-binding properties of cyclophane host [24]. Zaccheddu *et al.* [25] suggested the possibility of strengthening anion $\cdots \pi$ binding by $\pi \cdots \pi$ stacking interactions. Recent theoretical investigations have provided evidence for very favorable anion $\cdots \pi$ interactions occurring between charged aromatic compound – tropylium cation and various anions [26]. For substituted squaramide, the protonation of the pyridine ring enhances its electron-deficient character, which leads to shortening of anion $\cdots \pi$ contact distance [27]. Since the electrostatic term is greater than the polarization term [15], the combination of anion $\cdots \pi$ interactions with some additional binding interactions such as ion pairing should have significant role in modulating the anion-binding ability of receptors.

To probe the influence of additional ionic interactions on the strength of anion $\cdots \pi$ complex stability, crystallographic and computational studies have been performed on 5,6-membered fused-ring compounds with delocalized π-electron density [28] – 2-aminobenzothiazole (abt) supramolecular complexes. Different types of metal coordination compounds have been widely examined since they are promising candidates for efficient synthetic anion receptors or transporters [12, 14, 16, 29, 30]. The abt ligand was chosen because it is often used as a model for complex biologically active molecules [31] and due to the above-mentioned electronic properties.

Reaction of abt with iron(III) chloride or iron(III) ethanedioate leads to the formation of metal supramolecular complexes containing protonated ligand – 2-aminobenzothia-zolium ion (Habt) in the outer coordination sphere. One non-covalent interaction responsible for crystal packing is the anion $\cdots \pi$ interaction.

2. Experimental

2.1. *Synthesis of $2C_6H_4NHC(NH_2)S^+ \cdot [FeCl_4]^- \cdot Cl^- \cdot H_2O$ (1)*

FeOCl of 0.537 g (5 mmol) was dissolved in concentrated hydrochloric acid. The obtained solution was heated and then mixed with ethanolic solution of abt (1.5 g, 10 mmol; molar ratio 1 : 2). The solution was allowed to cool and stored at 275 K. After 1 week, orange crystals of **1** were formed.

2.2. *Synthesis of $3C_6H_4NHC(NH_2)S^+ \cdot [Fe(C_2O_4)_3]^{3-} \cdot 2H_2O$ (2)*

FeOCl of 0.537 g (5 mmol) was dissolved in saturated aqueous ethanedioic acid solution. The obtained solution was heated and then mixed with ethanolic solution of abt (1.5 g, 10 mmol; molar ratio 1 : 2). The solution was allowed to cool and stored at 275 K. After 1 day, yellow crystals of **2** were formed.

2.3. *X-ray crystallography*

The crystals were mounted on a KM-4-CCD automatic diffractometer equipped with a CCD detector for data collection. X-ray intensity data were collected with graphite-monochromated Mo-Kα radiation ($\lambda = 0.71073 \text{Å}$) at 291.0(3) K, with ω scan mode. A 18 s (**1**), 22 s (**2**) exposure time was used and reflections inside of the Ewald sphere were collected up to $2\theta = 50.0°$ (scan width 0.45°). The unit cell parameters were determined from 5771 (**1**), 3278 (**2**), the strongest reflections. Both crystals used for data collection did not change their appearance. Lorentz, polarization, and numerical absorption [32] corrections were applied to the measured data. The structures were solved by Patterson superposition procedure and subsequently completed by difference Fourier recycling. All non-hydrogen atoms were refined anisotropically using full-matrix, least-squares technique on F^2. The hydrogens were found on difference Fourier synthesis and treated as "riding" on their adjacent non-hydrogen atoms and assigned isotropic displacement parameters equal to 1.5 (amine groups, water molecules) or 1.2 (rest of atoms) times the value of equivalent displacement parameters of the parent atoms. The carbon-bonded hydrogen geometry was idealized after each cycle of least-squares refinement. SHELXS97, SHELXL97, and SHELXTL [33] programs were used for all the calculations. Atomic scattering factors were those incorporated in the computer programs. Details concerning crystal data and refinement are summarized in table 1; selected bond lengths and angles are given in table 2.

Table 1. Crystallographic data for **1** and **2**.

	$2C_6H_4NHC(NH_2)S^+ \cdot$ $[FeCl_4]^- \cdot Cl^- \cdot H_2O \cdot$ (**1**)	$3C_6H_4NHC(NH_2)S^+ \cdot$ $[Fe(C_2O_4)_3]^{3-} \cdot 2H_2O$ (**2**)
Compound		
Empirical formula	$C_{14}H_{16}Cl_5FeN_4OS_2$	$C_{27}H_{25}FeN_6O_{14}S_3$
Formula weight	553.53	809.56
Crystal system	Triclinic	Monoclinic
Space group	$P\bar{1}$	$P2_1/c$
Unit cell dimensions (Å, °)		
a	7.4228(3)	13.8564(17)
b	8.1655(3)	14.5180(18)
c	19.1070(5)	17.786(2)
α	86.432(2)	
β	84.740(3)	107.6920(10)
γ	84.627(3)	
Volume (Å^3), Z	1146.47(7), 2	3408.8(7), 4
Crystal size (mm^3)	$0.35 \times 0.21 \times 0.20$	$0.073 \times 0.003 \times 0.003$
Absorption coefficient (mm^{-1})	1.435	0.702
F (000)	558	1660
θ range for data collection (°)	2.14–25.00	1.85–25.05
Limiting indices	$-8 \leq h \leq 8$; $-9 \leq k \leq 9$; $-22 \leq l \leq 22$	$-16 \leq h \leq 16$; $-17 \leq k \leq 17$; $-21 \leq l \leq 21$
Goodness-of-fit on F^2	1.079	1.031
Final R indices [$I > 2\sigma(I)$]	$R_1 = 0.0274$, $wR_2 = 0.0727$	$R_1 = 0.0473$, $wR_2 = 0.1429$
R indices (all data)	$R_1 = 0.0338$, $wR_2 = 0.0761$	$R_1 = 0.0862$, $wR_2 = 0.1688$
Largest difference peak and hole (e Å^{-3})	0.533 and -0.485	0.623 and -0.558

Table 2. Selected geometrical parameters of **1** and **2**.

Bond length (Å)/angle (°)	**1**	Bond length (Å)/angle (°)	**2**
Fe1–Cl1	2.1945(7)	Fe1–O1	2.005(7)
Fe1–Cl2	2.1875(7)	Fe1–O3	1.946(7)
Fe1–Cl3	2.1844(8)	Fe1–O11	2.029(6)
Fe1–Cl4	2.1741(8)	Fe1–O13	2.029(5)
C1–S1	1.731(2)	Fe1–O21	2.043(5)
C2–S1	1.760(2)	Fe1–O23	2.009(6)
C11–S11	1.728(2)	C1–S1	1.732(10)
C12–S11	1.751(3)	C11–S11	1.749(10)
C2–C7	1.380(3)	C21–S21	1.720(10)
C12–C17	1.382(3)		
		N1–C1–S1	113.7(7)
N1–C1–S1	111.46(16)	N11–C11–S11	111.6(7)
C1–S1–C2	90.85(10)	N21–C21–S21	119.1(7)
N11–C11–S11	112.48(17)	C1–S1–C2	89.7(5)
C11–S11–C12	90.12(11)	C11–S11–C12	90.9(5)
		C21–S21–C22	87.9(4)

2.4. *Theoretical calculations*

All calculations were performed at the second-order Møller–Plesset (MP2) [34] level of theory using the 6-31++G(d,p) basis set by GAUSSIAN03 [35] program package. Basis set superposition error (BSSE) corrections were carried out using the counterpoise (CP) method of Boys and Bernardi [36]. Atomic charges were calculated according to natural population analysis (NPA) [37–39], Merz–Kollman–Singh (MKS) [40, 41],

and Breneman [42] schemes. Although calculation of effective atomic charges plays an important role in the application of quantum mechanical calculations to molecular systems, the unambiguous dividing up of the overall molecular charge density in atomic contributions is still an unresolved problem, and none of the known procedures give fully reliable values of atomic charges. Thus, a discussion of atomic charges should cover more than one algorithm used for charge density division. Generally, less reliable values are given by the Mulliken population analysis and more reliable results are provided by the Breneman method [43]. The natural bond orbital (NBO) [37–39] analysis has been employed to evaluate the stabilization energy of the donor–acceptor interactions. Density and potential contour plots were visualized with the gOpenMol program [44, 45].

2.5. *Spectroscopic, thermogravimetric, and X-ray powder diffractometric measurements*

IR spectra (400–4000 cm^{-1}) were taken in KBr discs in a Shimadzu DR-8011 spectrophotometer. UV-Vis spectra were recorded on a Jasco 660 spectrophotometer. Protonation constants were established using the DL-50 Graphix Titrator (Mettler–Toledo).

Thermal analyses were carried out in a TG/DTA-SETSYS-16/18 thermoanalyzer coupled with a ThermoStar (Balzers) mass spectrometer. The samples (6.45 mg for **1** and 5.65 mg for **2**) were heated in corundum crucibles up to 1000°C, at the heating rate 10°C min^{-1} in air. The products of decomposition were calculated from TG curves. The temperature ranges were determined by means of thermoanalyzer Data Processing Module [46]. A coupled TG-MS system was used to analyze the principal volatile thermal decomposition and fragmentation products. The final products of decomposition were determined by X-ray powder diffraction analysis. The samples were milled in the planetary ball corundum mill for 5 min, and then the X-ray powder diffraction patterns were measured in reflection mode on an XPert PRO X-ray powder diffraction system equipped with Bragg–Brentano PW 3050/65 high-resolution goniometer and PW 3011/20 proportional point detector. The Cu-Kα_1 radiation was used. The patterns were measured at 298.0 K in the range 5–90° with the narrowest beam attenuator (0.017 mm). The 6 s per 0.01° step procedure was used. The samples were sprinkled onto the sample holders using a small sieve to avoid a preferred orientation. The thicknesses of the samples were no more than 0.01 mm. During the measurements each specimen was spun in the specimen plane to improve particle statistics.

3. Results and discussion

3.1. *The description of the structures*

The crystal structure of **1** consists of two 2-aminobenzothiazolium cations, tetrachloroferrate(III) anion, chloride anion, and water molecule (figure 1). The coordination sphere geometry of the iron(III) atom can be described as a slightly distorted tetrahedron. The Fe–Cl bond lengths vary from 2.1741(8) to 2.1945(7) Å and are similar to those found for other tetrachloroferrates(III) compounds with aromatic
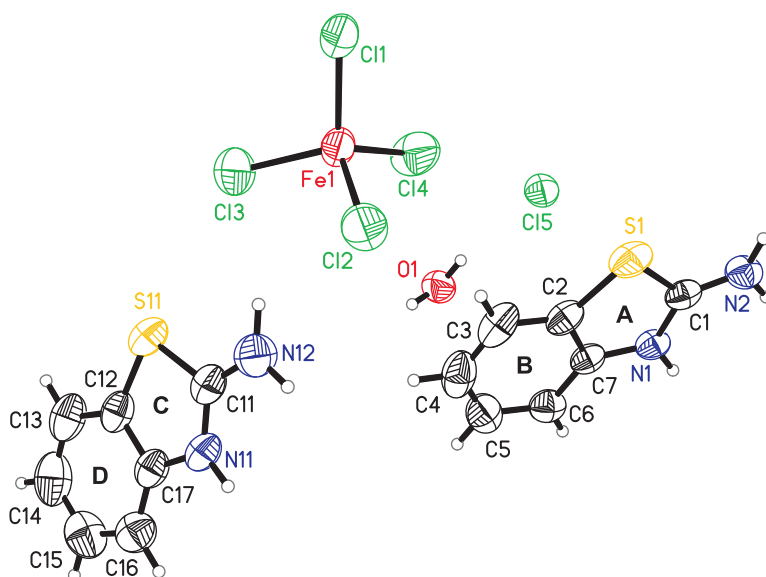
Figure 1.   The molecular structure of **1** showing the atom and ring numbering scheme. The displacement ellipsoids are drawn at 50% probability level and H atoms are shown as spheres of arbitrary radii.
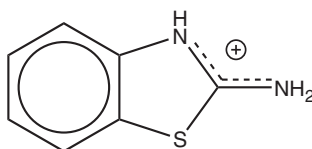

Figure 2.   The molecular drawing of Habt. The delocalized π-electron density among CN bonds is indicated by dashed lines.

nitrogen-containing organic bases [47–49]. The cations are slightly distorted from planarity, with the largest deviations from the weighted least-squares planes calculated through all non-H atoms of the cations equal to 0.0239(13) Å for N2 atom and 0.0066(13) Å for S11 atom. The bond lengths and angles of Habt are within the ranges reported for its complexes with inorganic anions [50, 51]. In both cations the endocyclic C–N bonds (1.334(2) Å for C1–N1 and 1.322(3) Å for C11–N11) are longer than the exocyclic C–NH$_2$ bonds (1.303(3) Å for C1–N2 and 1.314(3) Å for C11–N12). This suggests delocalization of electron density and, in consequence, delocalization of the positive charge over the N–C–NH$_2$ moiety (figure 2) [28]. To determine the multiplicity of the C–N bonds, the bond orders were calculated by the bond-valence method (BVM) [52, 53] using the Brown–Altermatt equation [54] $v_{ij} = \exp[(R_{ij} - d_{ij})/0.37]$. The bond-valence parameters R_{ij} taken as mean single-bond lengths were 1.47 and 1.35 Å for exocyclic C–N and endocyclic C–N bonds, respectively. The BVM bond orders are 1.04, 1.57 and 1.08, 1.53 v.u. (valence units), respectively, for the C1–N1, C1–N2 and C11–N11, C11–N12 bonds, which indicates a considerable degree of double-bond character between the exocyclic N and C.

Table 3. Hydrogen-bond geometry (Å, °) parameters for **1** and **2**.

D–H···A	D–H	H···A	D···A	D–H···A
1	0.90	2.22	3.1074(16)	167.8
N1–H1N···Cl5[i]	0.89	2.29	3.1583(18)	162.9
N2–H2N···Cl5[ii]	0.92	2.01	2.929(3)	176.4
N2–H2O···O1[i]	0.91	1.89	2.796(2)	177.0
N11–H11N···O1[iii]	0.93	2.42	3.340(2)	168.0
N12–H12N···Cl5[iii]	0.96	2.69	3.347(2)	126.9
N12–H12O···Cl2	0.96	2.82	3.673(2)	149.1
N12–H12O···Cl3	0.87	2.24	3.0189(16)	148.8
O1–H1O···Cl5	0.81	2.50	3.2792(17)	160.9
O1–H1P···Cl1[iv]				
2	0.86	2.24	2.968(11)	143.0
N1–H1···O24[v]	0.86	2.29	2.956(11)	134.3
N1–H1···O22[v]	0.83	1.98	2.809(11)	174.6
N2–H2N···O92[vi]	0.85	2.13	2.806(11)	136.8
N2–H2O···O22[v]	0.86	2.02	2.828(10)	156.1
N11–H11···O11[vi]	0.97	1.78	2.719(12)	160.8
N12–H12N···O91	0.90	2.07	2.932(11)	158.6
N12–H12O···O21[v]	0.90	2.46	3.100(11)	128.3
N12–H12O···O22[v]	0.86	2.01	2.846(10)	163.3
N21–H21···O13[vii]	0.99	1.85	2.818(11)	163.1
N22–H22N···O14[vii]	0.92	2.00	2.885(11)	162.3
N22–H22O···O12	0.87	2.06	2.914(11)	167.5
O91–H91O···O1[vi]	0.90	1.90	2.799(9)	178.4
O91–H91P···O23	0.97	2.11	3.064(10)	168.1
O92–H92O···O24[viii]	0.89	2.03	2.804(11)	144.8
O92–H92P···O2				

Symmetry codes: [i] −x+2, −y+1, −z; [ii] −x+1, −y+1, −z; [iii] x, y+1, z; [iv] x+1, y, z; [v] x, −y+½, z+½; [vi] −x+1, y−½, −z+½; [vii] −x+1, −y+1, −z+1; [viii] −x+1, y+½, −z+½.

The organic cations, tetrachloroferrate(III) anions, chloride anions, and water molecules of **1** are assembled *via* π···π stacking interactions, the H···π ring interactions, hydrogen bonds, and anion···π interactions into a 3-D supramolecular network. The π···π stacking interactions can be observed between benzene rings of adjacent, symmetry-related 2-aminobenzothiazolium ions oriented in opposite directions. The distances between centroids of rings are 3.754(5) Å for the CgB···CgB#(−x+2, −y+2, −z) interaction (CgB is the centroid of ring containing C2–C7) and 3.811(5) Å for the CgD···CgD#(−z+2, −y+3, −z+1) interaction (CgD is the centroid of ring containing C12–C17); the perpendicular distances between the ring centroid and ring plane are 3.370(5) and 3.670(5) Å, respectively. Angles between the vector linking one ring centroid and the normal to the second ring plane are 26.2(4) and 15.7(4)°, respectively, as above. An interesting feature is the presence of two weak O–H···π ring interactions: O1–H1O···CgB with H···CgB distance of 3.306 Å, O···CgB distance of 3.540 Å, O–H···CgB angle of 98.50° and O1–H1P···CgB with H···CgB distance of 3.391 Å, O···CgB distance of 3.540 Å, O–H···CgB angle of 93.96°.

The arrangement of cations, anions, and neutral molecules in the structure is also governed by a 3-D network of N–H···Cl hydrogen bonds between Habt molecules and outer coordination sphere chloride ion and chloride ions coordinated to Fe atom, the N–H···O hydrogen bonds between the Habt molecules and water molecules, the O–H···Cl hydrogen bonds between water molecules and outer coordination sphere
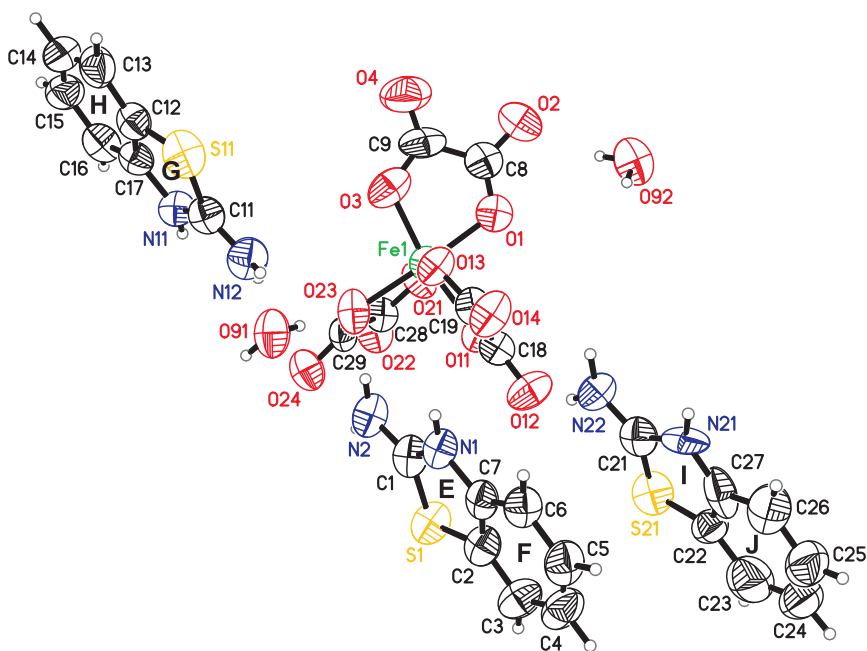
Figure 3. The molecular structure of **2** showing the atom and ring numbering scheme. The displacement ellipsoids are drawn at 50% probability level and H atoms are shown as spheres of arbitrary radii.
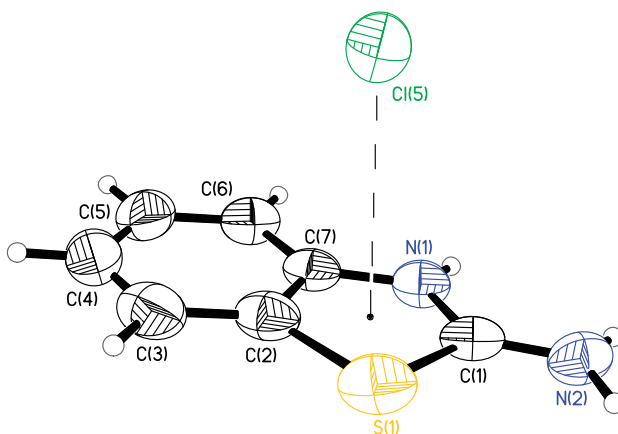
Figure 4. Anion $\cdots \pi$ interaction in **1A**.

chloride ion and chloride ions of tetrachloroferrate ion. Hydrogen-bond geometrical parameters are presented in table 3.

The crystal structure of **2** contains three 2-aminobenzothiazolium cations as counterions, balancing the charge of triethanedioatoferrate(III) anion, and two water molecules (figure 3). The ethanedioate groups are coordinated to iron in bidentate chelating mode and each carboxylate group is monodentate. According to Cambridge

Structural Database (CSD, Version 5.30 [55]) such coordination is less common than tetradentate bridging–chelating. The coordination environment of iron(III) atom adopts a *trans*-distorted tetragonal bipyramid. The cations are slightly distorted from planarity, with the largest deviations from the weighted least-squares planes calculated through all non-H atoms of each cation existing for C5 [0.021(8) Å], S11 [0.042(5) Å], and C24 [0.025(9) Å]. Similar to **1**, the π-electron density is delocalized over the N–C–NH_2 moiety in Habt. The bond lengths of endocyclic C–N bonds are 1.307(11) Å for C1–N1, 1.316(11) Å for C11–N11, and 1.332(11) Å for C21–N21, whereas the exocyclic C–NH_2 bonds are 1.334(11) Å for C1–N2, 1.291(11) Å for C11–N12, and 1.372(11) Å for C21–N22, respectively. In one Habt molecule (containing S11 atom) the C–NH_2 bond is slightly shorter than the C–N bond, in the two remaining molecules the C–NH_2 bonds are longer than the C–N bonds. The BVM bond orders [52–54] (calculated as above) also imply the π-character of these exocyclic C–NH_2 bonds. The BVM bond orders are then 1.12, 1.44, 1.10, 1.62 and 1.05, 1.30 v.u., respectively, for the C1–N1, C1–N2, C11–N11, C11–N12 and C21–N21, C21–N22 bonds. In the third Habt molecule (N21, N22, S21, C22–C27) the C–S bonds are shorter than in two remaining molecules (table 2), suggesting localization of electron density in the 2-aminothiazole ring.

The cations and complex anions are arranged in layers along crystallographic *b0c* plane, and within each cationic layer the ions are connected along the crystallographic *b*-axis *via* $\pi \cdots \pi$ stacking interactions. The $\pi \cdots \pi$ stacking interactions can be observed between benzene rings and thiazole ring of almost parallel 2-aminobenzothiazolium ions oriented in the same direction. The distances between centroids of rings are 3.954(6) Å for the CgE$\cdots Cg$H#$(-x+1, -y, -z+1)$ interaction, 3.757(5) Å for the CgF$\cdots Cg$I interaction, and 3.889(6) Å for the CgG$\cdots Cg$J#$(-x+1, -y+1, -z+1)$ interaction (CgE, CgF, CgG, CgH, CgI, CgJ means centroids of rings containing C2–S1, C2–C7, C12–S11, C12–C17, C22–S21, C22–C27, respectively), and the perpendicular distances between the ring centroids and ring planes are 3.421(5), 3.559(5), and 3.444(4) Å, respectively. The angles between the vector linking the one ring centroids and the normal to the second ring plane are 30.1(5), 18.7(4), and 27.7(6)°, respectively, as above. Habt molecules and triethanedioatoferrate(III) ions are connected by imine/amine-carboxylate N–H$\cdots$O hydrogen bonds (table 3) and ethanedioate$\cdots\pi$ interactions. Such bonds are also formed between Habt molecules and water molecules. Additionally, complex anions are linked with water molecules by O–H$\cdots$O hydrogen bonds, forming a zigzag chain along the *b*-axis. Each cationic layer consists of two sublayers composed from cations arranged in opposite directions (aromatic ring to aromatic ring) and joined by the C–H$\cdots\pi$ interactions (C4–H2$\cdots Cg$H with H$\cdots Cg$H distance of 3.086 Å, C$\cdots Cg$H distance of 3.883 Å, C–H$\cdots Cg$H angle of 144.8°).

3.2. *Structural and theoretical investigations of the anion-π interaction*

Compound **1** shows evidence of anion$\cdots\pi$ interaction (figure 4). The non-coordinated chloride ion interacts with the thiazole ring (CgA) of Habt molecule (containing S1 atom, **1A**). The Cl5$\cdots Cg$A distance is 3.715 Å and the angle of the Cl5$\cdots$centroid vector to the ring plane is 79.5°. Despite many theoretical and crystallographic investigations concerning the interactions of anions with six-membered aromatic rings there is no
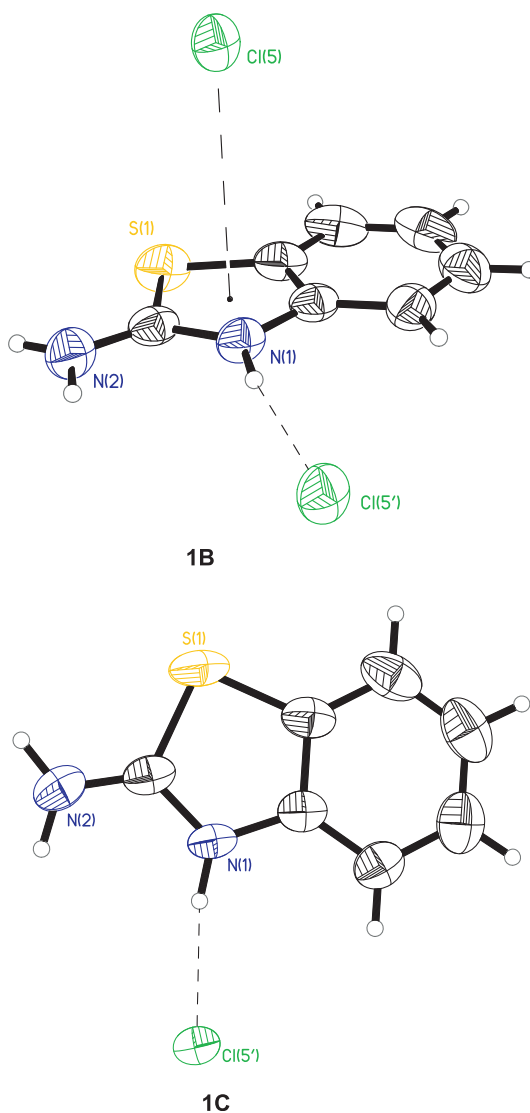
1B

1C

Figure 5. Fragments of molecule **1** used for the theoretical calculations of the chloride$\cdots\pi$ interaction energy. The primed atom was obtained by symmetry transformation $-x+2$, $-y+1$, $-z$.

systematic research on anion$\cdots\pi$ contacts involving five-membered rings. Such studies have been performed only for cyclopentadienyl ring in $[\eta^5\text{-Cp-Me}]^+$ systems [56]. Utilizing the method of interaction strength determination, which has been proposed for six-membered aromatic rings [57], this chloride$\cdots\pi$ interaction (involving five-membered heterocyclic ring) is rather weak. This distance is above the sum of Cl ionic radius and N, C, S van der Waals radii (equal to 3.36, 3.51, 3.61 Å [58, 59], respectively). The distances are longer than those observed between rings possessing protonated nitrogen – pyridinium ring and metal coordinated or free chlorides in $(C_{18}H_{14}N_2)Cl_2 \cdot 2H_2O$, $(C_{16}H_{12}N_4)Cl_2 \cdot 2H_2O$, and $(C_{16}H_{13}N_4)[CoCl_4]Cl$ [60]. In **2**, the organic anion shows greater tendency to form hydrogen bonds than anion$\cdots\pi$ contacts.

Quantum-mechanical calculations have been carried out on the isolated organic cation–anion fragment (figure 4) to confirm the presence of the bonding anion$\cdots\pi$ interaction. The geometric parameters were employed from the crystal structure data. The geometry was not optimized. The total interaction energy (with the BSSE corrections) of $-71.37\,\mathrm{kcal\,mol^{-1}}$ indicates that the formation of contacts between anions and rings of charged organic molecules is favorable.

According to Hay and Bryantsev [61] geometric parameters are not sufficient evidence for anion$\cdots\pi$ interactions. Anions can interact with aromatic systems also by weakly covalent σ interactions and strongly covalent σ interactions. Thus, the non-covalent nature of bonding interactions in the compounds was analyzed by the NBO method [37–39]. In this method the strength of the donor–acceptor charge-transfer delocalization is characterized by the second-order stabilization energy, ΔE. In **1**, charge-transfer interactions occur between the chloride lone pairs and antibonding orbitals of π-systems. The stabilization energy is equal to $0.8\,\mathrm{kcal\,mol^{-1}}$ for the Cl5–CgA interaction in **1A**. Generally, the charge transfer is larger in the case of more charge-dense inorganic anions and smaller for charge-diffuse organic anions. ΔE less than $1\,\mathrm{kcal\,mol^{-1}}$ confirms the predominantly non-covalent nature of interaction and small contribution of charge transfer to the total interaction energy.

The contribution of ion-pair interaction energy to the total binding energy was calculated for the chloride ion–benzothiazolium ion system (**1A**). By adding the additional chloride ion to **1A** the fragment **1B** was formed, in which an additional hydrogen-bonding interaction exists between charged species (figure 5). The total binding energy of **1B** is $-112.2\,\mathrm{kcal\,mol^{-1}}$. The energy of benzothiazolium ion interacting with chloride ion through the hydrogen bond (**1C**) was also calculated. The binding energy is $-95.7\,\mathrm{kcal\,mol^{-1}}$. The difference between these binding energies of **1B** and **1C** could be considered as the anion$\cdots\pi$ energy contribution equal to $-16.5\,\mathrm{kcal\,mol^{-1}}$. This confirms the existence of this interaction, although the geometrical parameters are not common (they are different from those established on the basis of quantum-mechanical calculations performed for model compounds). Similar energy was obtained for the squaramide–nitrate salt calculated at the RI-MP2/6-31++G** level of theory [27]. In all cases the geometry was not optimized and the energy was BSSE corrected. The ion-pair interaction energy was derived by subtracting the interaction energy of anion$\cdots\pi$ contact from the interaction energy of **1A**. The contribution of ion-pair interaction energy is $-54.9\,\mathrm{kcal\,mol^{-1}}$, roughly 77% of total binding energy.

The character of interaction can be also proved by electron charge density at the bond critical point, $\rho(r_C)$ [62]. The covalent bond carries a density higher than $0.1\,\mathrm{e\,\AA^{-3}}$ at the critical point while the non-covalent bond exhibits much lower density at the critical point. Since $\rho(r_C)$ can be compared with the maximum density in the region between two interacting moieties (ρ_{max}) [61], as an example the electron density isosurfaces have been presented for **1A** (figure 6). At isosurface values less than $0.005\,\mathrm{e\,\AA^{-3}}$, a concentration of electron density between Cl$^-$ and Habt can be observed. At isosurface values greater than $0.005\,\mathrm{e\,\AA^{-3}}$, the electron density surfaces are discontinuous between Cl$^-$ and Habt. Thus, **1A** exhibits a ρ_{max} of $0.005\,\mathrm{e\,\AA^{-3}}$, indicating the non-covalent character of intramolecular interaction between the anion and organic ligand. The similar order of magnitude of ρ_{max} has been observed for anion$\cdots\pi$ interaction in the 1,3,5-triazine-bromide system [61].
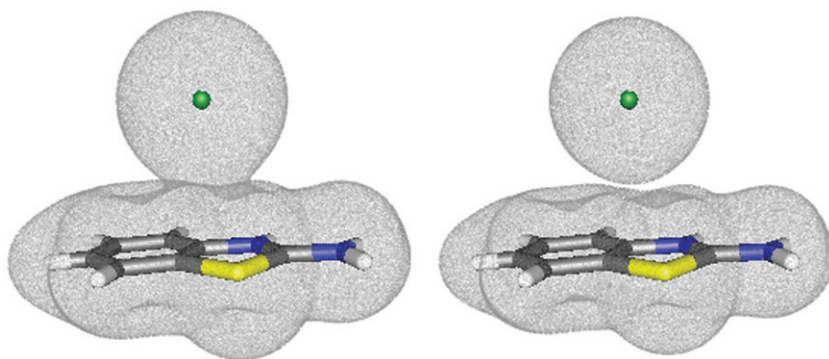
Figure 6. Electron density surfaces for value of 0.004 (left) and 0.006 (right) e Å^{-3} of **1A**.

Table 4. The atomic charges calculated for **1** and **2**.

Compound	Atom/group	MKS charge	Breneman charge	NPA charge
1	N12	−1.003	−0.998	−0.800
	N11	−0.435	−0.627	−0.586
	N12H$_2$	0.051	0.006	0.068
	S11	0.072	0.005	0.495
	*Cg*C	0.681	0.663	0.727
	N2	−0.587	−0.650	−0.765
	N1	−0.046	−0.295	−0.585
	N2H$_2$	0.222	0.133	0.069
	S1	0.138	0.011	0.515
	*Cg*A	0.446	0.644	0.771
2	N2	−1.715	−1.747	−0.820
	N1	−0.913	−0.998	−0.629
	N2H$_2$	−0.273	−0.360	−0.091
	S1	−0.284	−0.353	0.308
	*Cg*E	0.486	0.571	0.199
	N12	−1.090	−1.041	−0.799
	N11	−0.336	−0.478	−0.539
	N12H$_2$	−0.005	−0.017	0.074
	S11	−0.169	−0.175	0.400
	*Cg*G	0.788	0.815	0.812

The charge distribution in Habt molecules forming anion$\cdots\pi$ interactions, hydrogen bonds, and stacking interactions is different in **1** and **2** (table 4). Generally, the endocyclic and exocyclic *N* atoms are negatively charged and, as expected, the exocyclic *N* atoms have bigger negative charges. In Habt of **2**, parts with negative (amine group) and positive (5-membered ring) net charge can be distinguished. In Habt of **1**, the amine groups are positively charged.

3.3. *Protonation constant*

Protonation constants of abt were determined potentiometrically in ethanol–water mixture containing 10% ethanol (v/v). Titration was performed at 25°C and the ionic strength of the medium was maintained at 0.10 mol dm^{-3} using sodium chloride. The

$\log K_1$ is equal to 7.06 ± 0.12 and $\log K_2$ is equal to 6.66 ± 0.10. The first protonation constant is related to the protonation of nitrogen atom in the amine and the second corresponds to the protonation of nitrogen atom in the thiazole ring.

3.4. Spectroscopic studies

IR spectra of **1** and **2** (figures S1 and S2 of the "Supplementary material") contain characteristic bands of stretching vibrations of NH_2, NH, OH, and CH at 3050–3415 cm^{-1}. The wide split absorption band at 1635–1690 cm^{-1} is attributed to the δNH_2, $\nu C=N$ vibrations of organic ligand, bending vibrations of OH, and asymmetric stretching of CO in **2** [63]. The bands around 1580 and 1470 cm^{-1} confirm the presence of aromatic CC bonds. A strong band observed at 1260 cm^{-1} is assigned to exocyclic CN stretching vibrations and NH bending vibrations. The medium intensity band at 640 cm^{-1} corresponds to the vibrations of thiazolium C–S. Additionally, the IR spectrum of **2** showed a strong band at 1392 cm^{-1} originating from the symmetric stretch of CO bonds of bidentate ethanedioate [64, 65]. The νCC modes are assigned to 890 and 803 cm^{-1}. The CO_2 deformation vibrations are also identified in IR spectra between 490 and 534 cm^{-1}.

UV-Vis spectra were recorded in DMF solution (figures S3 and S4 of the "Supplementary material"). The spectrum of **1** in ethanol–water mixture (25% ethanol, v/v) was also obtained (figure S5 of the "Supplementary material"). Compound **2** is insoluble in water, ethanol, and all other common solvents.

The UV-Vis spectrum of **1** in the ethanol–water mixture exhibits six bands. Strong, sharp bands at 203 ($\varepsilon = 4790$ m^2 mol^{-1}) and 221 nm ($\varepsilon = 4730$ m^2 mol^{-1}) are attributed to $\pi \rightarrow \pi^*$ transitions of Habt. The broad band at 260 nm ($\varepsilon = 2010$ m^2 mol^{-1}) with a shoulder at 286 nm ($\varepsilon = 1050$ m^2 mol^{-1}) are $n \rightarrow \pi^*$ transitions of Habt. The relatively low-intensity bands present at 345 ($\varepsilon = 131$ m^2 mol^{-1}) and 418 nm ($\varepsilon = 10$ m^2 mol^{-1}) are charge-transfer ligand to the metal electronic transitions.

The electronic spectrum of **1** in DMF is dominated by three bands at 300 ($\varepsilon = 1010$ m^2 mol^{-1}), 322 ($\varepsilon = 687$ m^2 mol^{-1}), and 364 nm ($\varepsilon = 454$ m^2 mol^{-1}) assigned to $n \rightarrow \pi^*$ transitions of Habt ligand and the two characteristic charge-transfer transitions from Cl$^-$ to Fe(III), respectively. For **2**, absorption feature ascribed to $n \rightarrow \pi^*$ transitions of organic ligand is observed at 300 nm ($\varepsilon = 102$ m^2 mol^{-1}).

3.5. Thermal studies

Compound **1** is thermally stable to 50°C (figure S6 of the "Supplementary material"). The decomposition is a multi-stage process. The first endothermic step of thermal decomposition occurs from 50°C to 140°C. The initial mass loss is attributed to the removal of water. The next step of decomposition is characterized by two broad peaks on the DTG curve at 210°C and 255°C that cannot be distinguished from the TG curve. The three following steps are exothermic with mass losses of 28% (with minimum on DTG at 350°C), 17% (with minimum on DTG at 460°C), and 34% (with minimum on DTG at 550°C), respectively. According to the detected gaseous products, in the range 140–600°C the multi-stage combined decomposition of the protonated organic cations, tetrachloroferrate(III) anions, and chloride anions begins simultaneously. The main volatile products come from Habt decomposition (figure S7 of the "Supplementary material"). The mass spectrum (MS) of the thermal decomposition shows ion current

signals $m/z = 30$, 43, 44, 46, 64, and 76 which correspond to the molecular masses of NO^+, $CN_2H_3^+$, CO_2^+ and/or SC^+, NO_2^+, SO_2^+, and $C_6H_4^+$. The MS does not display the presence of Cl_2 ($m/z = 70$, 72) or HCl ($m/z = 35$, 37). During thermal decomposition chlorides probably form volatile organic chlorides. A similar degradation pattern has been observed for tetrabutylammonium tetrachloroferrate(III) [66]. Over 600°C, **1** decomposes to α-Fe_2O_3. The final product of decomposition was confirmed by X-ray powder diffraction analysis (figure S8 of the "Supplementary material").

Complex **2** is stable to 50°C and its decomposition is a four-stage process (figure S9 of the "Supplementary material"). From 50°C to 140°C water molecules are released from the outer coordination sphere. In the DTA curve such dehydration appears as an endothermic peak. All succeeding steps are exothermic and are attributed to decomposition of Habt and ethanedioate ions. The DTA and DTG curves exhibit three peaks at 215°C (with mass loss of 36%), 350°C (with mass loss of 7%), and 450°C (with mass loss of 24%), respectively. Over 500°C, **2** also decomposes to α-Fe_2O_3, confirmed by X-ray powder diffraction analysis (figure S8 of the "Supplementary material"). The main volatile products of decomposition and fragmentation processes from 160 to 580°C include C^+ ($m/z = 12$), NO^+ ($m/z = 30$), CO_2^+ and/or SC^+ ($m/z = 44$), NO_2^+ ($m/z = 46$) and $SCNH_2^+$ ($m/z = 60$) (figure S10 of the "Supplementary material").

4. Summary

The principal interactions controlling the structures of **1** and **2** are hydrogen bonds and stacking interactions. Compound **1** shows evidence of interactions that can be classified as anion$\cdots\pi$ interactions. The interaction between non-coordinated chloride ion and 2-aminobenzothiazolium cations is characterized by long distances with strength typical for ion-pair interactions and the directionality characteristic for anion$\cdots\pi$ interactions. Although the existence of anion$\cdots\pi$ interactions is questionable [67], in the present case the results of quantum-mechanical calculations indicate that the chloride ion and thiazolium ring are connected not only by electrostatic interaction but also by bonding interaction, which can be considered as anion$\cdots\pi$ contact. Since protonation is a common process occurring in physiological systems and almost all drugs or bioactive molecules undergo protonation before they enter the reaction chain, the effect of non-covalent interactions such as ion-pairing and anion$\cdots\pi$ interactions can be important and might help to design anion receptors [68, 69].

Supplementary material

Acknowledgments

References

[1] S. Kubik, C. Reyheller, S. Stüwe. *J. Incl. Phenom. Macrocycl. Chem.*, **52**, 137 (2005).

[2] P.D. Beer, P.A. Gale. *Angew. Chem. Int. Ed.*, **40**, 486 (2001).

[3] T. Gunnlaugsson, M. Glynn, G.M. Tocci, P.E. Kruger, F.M. Pfeffer. *Coord. Rev. Chem.*, **250**, 3094 (2006).

[4] C. Caltagirone, P.A. Gale. *Chem. Soc. Rev.*, **38**, 520 (2009).

[5] S.O. Kang, R.A. Begum, K. Bowman-James. *Angew. Chem. Int. Ed.*, **45**, 7882 (2006).

[6] E. Kimura, S. Aoki, T. Koike, M. Shiro. *J. Am. Chem. Soc.*, **119**, 3068 (1997).

[7] E.J. O'Neil, B.D. Smith. *Coord. Rev. Chem.*, **250**, 3068 (2006).

[8] J.W. Steed. *Chem. Soc. Rev.*, **38**, 506 (2009).

[9] T.H. Kwon, K.-S. Jeong. *Tetrahedron Lett.*, **47**, 8539 (2006).

[10] D. Quiñonero, C. Garau, C. Rotger, A. Frontera, P. Ballester, A. Costa, P.M. Deyà. *Angew. Chem. Int. Ed.*, **41**, 3389 (2002).

[11] K. Hiraoka, S. Mizuse, S. Yamabe. *J. Phys. Chem.*, **91**, 5294 (1987).

[12] P. Gamez, T.J. Mooibroek, S.J. Teat, J. Reedijk. *Acc. Chem. Res.*, **40**, 435 (2007).

[13] B.P. Hay, V.S. Bryantsev. *Chem. Commun.*, 2417 (2008).

[14] B.L. Schottel, H.T. Chifotides, K.R. Dunbar. *Chem. Soc. Rev.*, **37**, 68 (2008).

[15] C. Garau, A. Frontera, D. Quiñonero, P. Ballester, A. Costa, P.M. Deyà. *Chem. Phys. Lett.*, **392**, 85 (2004).

[16] S. Demeshko, S. Dechert, F. Meyer. *J. Am. Chem. Soc.*, **126**, 4508 (2004).

[17] C. Garau, A. Frontera, P. Ballester, D. Quiñonero, A. Costa, P.M. Deyà. *Eur. J. Org. Chem.*, 179 (2005).

[18] A. Clements, M. Lewis. *J. Phys. Chem. A*, **110**, 12705 (2006).

[19] C. Garau, D. Quiñonero, A. Frontera, P. Ballester, A. Costa, P.M. Deyà. *New J. Chem.*, **27**, 211 (2003).

[20] O.B. Berryman, V.S. Bryantsev, D.P. Stay, D.W. Johnson, B.P. Hay. *J. Am. Chem. Soc.*, **129**, 48 (2007).

[21] C. Garau, D. Quiñonero, A. Frontera, P. Ballester, A. Costa, P.M. Deyà. *J. Phys. Chem. A*, **109**, 9341 (2005).

[22] B.L. Schottel, H.T. Chifotides, M. Shatruk, A. Chouai, L.M. Pérez, J. Bacsa, K.R. Dunbar. *J. Am. Chem. Soc.*, **128**, 5895 (2006).

[23] H. Maeda, A. Osuka, H. Furuta. *J. Incl. Phenom. Macrocycl. Chem.*, **49**, 33 (2004).

[24] S.M. Ngola, P.C. Kearney, S. Mecozzi, K. Russell, D.A. Dougherty. *J. Am. Chem. Soc.*, **121**, 1192 (1999).

[25] M. Zaccheddu, C. Filippi, F. Buda. *J. Phys. Chem. A*, **112**, 1627 (2008).

[26] D. Quiñonero, A. Frontera, D. Escudero, P. Ballester, A. Costa, P.M. Deyà. *ChemPhysChem*, **8**, 1182 (2007).

[27] C. Rotger, B. Soberats, D. Quiñonero, A. Frontera, P. Ballester, J. Benet-Buchholz, P. Ballester, A. Costa. *Eur. J. Org. Chem.*, 1864 (2008).

[28] A. Trzesowska-Kruszynska, R. Kruszynski. *Acta Crystallogr.*, **C65**, o19 (2009).

[29] L.A. Barrios, G. Aromí, A. Frontera, D. Quiñonero, P.M. Deyà, P. Gamez, O. Roubeau, E.J. Shotton, S.J. Teat. *Inorg. Chem.*, **47**, 5873 (2008).

[30] S.R. Choudhury, C.-Y. Chen, S. Seth, T. Kar, H.M. Lee, E. Colacio, S. Mukhopadhyay. *J. Coord. Chem.*, **62**, 540 (2009).

[31] I.I. Padilla-Martínez, E.V. García-Báez, H. Höpfl, F.J.I. Martínez-Martínez. *Acta Crystallogr.*, **C59**, o544 (2003).

[32] *X-RED* (*Version 1.18*). STOE & Cie GmbH, Darmstadt, Germany (1999).

[33] G.M. Sheldrick. *Acta Crystallogr.*, **A64**, 112 (2008).

[34] M. Head-Gordon, T. Head-Gordon. *Chem. Phys. Lett.*, **220**, 122 (1994).

[35] M.J. Frisch, G.W. Trucks, H.B. Schlegel, G.E. Scuseria, M.A. Robb, J.R. Cheeseman, J.A. Montgomery Jr, T. Vreven, K.N. Kudin, J.C. Burant, J.M. Millam, S.S. Iyengar, J. Tomasi, V. Barone, B. Mennucci, M. Cossi, G. Scalmani, N. Rega, G.A. Petersson, H. Nakatsuji, M. Hada, M. Ehara, K. Toyota, R. Fukuda, J. Hasegawa, M. Ishida, T. Nakajima, Y. Honda, O. Kitao, H. Nakai, M. Klene, X. Li, J.E. Knox, H.P. Hratchian, J.B. Cross, V. Bakken, C. Adamo, J. Jaramillo, R. Gomperts, R.E. Stratmann, O. Yazyev, A.J. Austin, R. Cammi, C. Pomelli, J.W. Ochterski, P.Y. Ayala, K. Morokuma, G.A. Voth, P. Salvador, J.J. Dannenberg, V.G. Zakrzewski, S. Dapprich, A.D. Daniels, M.C. Strain, O. Farkas, D.K. Malick, A.D. Rabuck, K. Raghavachari, J.B. Foresman, J.V. Ortiz, Q. Cui, A.G. Baboul, S. Clifford,

J. Cioslowski, B.B. Stefanov, G. Liu, A. Liashenko, P. Piskorz, I. Komaromi, R.L. Martin, D.J. Fox, T. Keith, M.A. Al-Laham, C.Y. Peng, A. Nanayakkara, M. Challacombe, P.M. W. Gill, B. Johnson, W. Chen, M.W. Wong, C. Gonzalez, J.A. Pople. Gaussian 03, Revision E.01, Gaussian, Inc., Wallingford CT (2004).

[36] S.F. Boys, F. Bernardi. *Mol. Phys.*, **19**, 553 (1970).
[37] A.E. Reed, L.A. Curtis, F.A. Weinhold. *Chem. Rev.*, **88**, 899 (1988).
[38] J.P. Foster, F.A. Weinhold. *J. Am. Chem. Soc.*, **102**, 7211 (1980).
[39] A.E. Reed, F.A. Weinhold. *J. Chem. Phys.*, **83**, 1736 (1985).
[40] U.C. Singh, P.A. Kollman. *J. Comput. Chem.*, **5**, 129 (1984).
[41] B.H. Besler, K.M. Merz Jr, P.A. Kollman. *J. Comput. Chem.*, **11**, 431 (1990).
[42] C.M. Breneman, K.B. Wiberg. *J. Comput. Chem.*, **11**, 361 (1990).
[43] F. Martin, H. Zipse. *J. Comput. Chem.*, **26**, 97 (2005).
[44] L. Laaksonen. *J. Mol. Graph.*, **10**, 33 (1992).
[45] D.L. Bergman, L. Laaksonen, A. Laaksonen. *J. Mol. Graph. Model.*, **15**, 301 (1997).
[46] Data processing Module, Copyright © 1994-1998 SETARAM – FRANCE; Version 1.4.
[47] D. Wyrzykowski, Z. Warnke, R. Kruszyński, J. Kłak, J. Mroziński. *Transition Met. Chem.*, **31**, 765 (2006).
[48] F. Zordan, S.L. Purver, H. Adams, L. Brammer. *CrystEngComm*, **7**, 350 (2005).
[49] J.-C. Daran, Y. Jeannin, L.M. Martin. *Acta Crystallogr.*, **B35**, 3030 (1979).
[50] L. Antolini, A. Benedetti, A.C. Fabretti, A. Giusti. *Inorg. Chem.*, **27**, 2192 (1988).
[51] Z. García-Hernández, A. Flores-Parra, J.M. Grevy, A. Ramos-Organillo, R. Contreras. *Polyhedron*, **25**, 1662 (2006).
[52] I.D. Brown. *The Chemical Bond in Inorganic Chemistry: The Bond Valence Model*, Oxford University Press, New York (2002).
[53] F. Mohri. *Acta Crystallogr.*, **B56**, 626 (2000).
[54] I.D. Brown, D. Altermatt. *Acta Crystallogr.*, **B41**, 244 (1985).
[55] F.H. Allen. *Acta Crystallogr.*, **B58**, 380 (2002).
[56] C. Garau, A. Frontera, D. Quiñonero, P. Ballester, A. Costa, P.M. Deyà. *Chem. Phys. Lett.*, **382**, 534 (2003).
[57] T.J. Mooibroek, C.A. Black, P. Gamez, J. Reedijk. *Cryst. Growth Des.*, **8**, 1082 (2008).
[58] R.D. Shannon. *Acta Crystallogr.*, **A32**, 751 (1976).
[59] A.J. Bondi. *Phys. Chem.*, **68**, 441 (1964).
[60] T. Dorn, C. Janiak, K. Abu-Shandi. *CrystEngComm*, **7**, 633 (2005).
[61] B.P. Hay, V.S. Bryantsev. *Chem. Commun.*, 2417 (2008).
[62] S.J. Grabowski, W.A. Sokalski, E. Dyguda, J. Leszczyński. *J. Phys. Chem. B*, **110**, 6444 (2006).
[63] E. Koglin, E.G. Witte, R.J. Meier. *Vib. Spectrosc.*, **33**, 49 (2003).
[64] M. del Arco, S. Gutiérrez, C. Martín, V. Rives. *Inorg. Chem.*, **42**, 4232 (2003).
[65] H.G.M. Edwards, N.C. Russell. *J. Mol. Struct.*, **443**, 223 (1998).
[66] D. Wyrzykowski, T. Maniecki, A. Pattek-Janczyk, J. Stanek, Z. Warnke. *Thermochim. Acta*, **435**, 92 (2005).
[67] B.P. Hay, R. Custelcean. *Cryst. Growth Des.*, **9**, 2539 (2009).
[68] J. Li, H. Lin, H. Lin. *J. Coord. Chem.*, **62**, 1921 (2009).
[69] B.I. Kharisov, P. Elizondo Martnez, V.M. Jimnez-Prez, O.V. Kharissova, B. Njera Martnez, N. Prez. *J. Coord. Chem.*, **63**, 1 (2010).